ELSEVIER

Earth and Planetary Science Letters 172 (1999) 97–109

EPSL

www.elsevier.com/locate/epsl

# In situ origin for glass in mantle xenoliths from southeastern Australia: insights from trace element compositions of glasses and metasomatic phases

Gregory M. Yaxley [a,*], Vadim Kamenetsky [b]

[a] *Research School of Earth Sciences, The Australian National University, Canberra, ACT 0200, Australia*
[b] *School of Earth Sciences and Centre for Ore Deposit Research, University of Tasmania, G.P.O. Box 252-79, Hobart, TAS, Australia*

Received 27 October 1998; revised version received 12 July 1999; accepted 29 July 1999

**Abstract**

Siliceous, aluminous and alkali-rich glasses, commonly found in patches and veins in spinel peridotite xenoliths, have been attributed to a number of different origins. These include low-degree primary melts of the mantle, exotic metasomatic melts influxing into the lithosphere, or breakdown of amphibole, and other phases during high-temperature transport of the xenoliths to the surface in their host magmas. We present new laser ablation–inductively coupled plasma–mass spectrometry (LA–ICP–MS) analyses of trace element abundances in glasses, and in metasomatically introduced phases (clinopyroxene, amphibole, phlogopite, apatite) from a suite of spinel wehrlite, lherzolite and harzburgite xenoliths from southeastern Australia. The majority of glass compositions are best explained by melting of amphibole (usually complete, as amphibole is now absent from most samples) with varying but significant contributions from partial melting of clinopyroxene. However, some glasses require additional components derived from partial or complete modal melting of phlogopite, or apatite. The data confirm our earlier model, that the glass present in patches in these samples derives from high-temperature, transport-related breakdown of a metasomatic phase assemblage (amphibole + clinopyroxene ± phlogopite ± apatite) present in the xenoliths prior to their entrainment in the host magmas. 

*Keywords:* xenoliths; trace elements; glasses; metasomatism; south Australia

## 1. Introduction

Mantle-derived spinel peridotite xenoliths, brought to the surface in alkali basaltic eruptions, often contain patches, veinlets and inclusions of siliceous, aluminous, alkali-rich glass located interstitially to primary phases (e.g. [1–6]). Draper and Green [7] have reported the compositional range exhibited by a comprehensive database of worldwide xenolith glass analyses. The glasses contain from 40 to >70 wt% $SiO_2$, up to 12 wt% $Na_2O$, up to 10 wt% $K_2O$ and up to 25 wt% $Al_2O_3$. MgO, FeO and CaO contents are low. As a result, the glasses range from strongly nepheline-normative to strongly quartz-normative compositions, and almost always contain distinctly low normative olivine and diopside. In recent years, the interpretation of the origin(s) of these

* Corresponding author. Current address: Institut für Mineralogie, Universität Frankfurt, Seckenberganlage 28, 60054 Frankfurt/M, Germany. Tel.: +49-69-798-23501; Fax: +49-69-798-28066; E-mail: yaxley@em.uni-frankfurt.de

0012-821X/99/$ – see front matter 
PII: S0012-821X(99)00196-X

glassy patches and veinlets has remained controversial, with a number of models being proposed. It has been suggested that the glasses are the result of (1) low-degree partial melting of the mantle [7–9], (2) interactions between invading basaltic melts and lithospheric phases (e.g. [5,10,11]), (3) partial melting of the lithosphere induced by influxing metasomatic fluids or melts [12], (4) migrating metasomatic melts in the lithosphere [7,13–15], or (5) partial or complete breakdown of metasomatically introduced phases such as amphibole, phlogopite, apatite, and sometimes clinopyroxene, shortly prior to, or during transport of the xenoliths to the surface in the host magma [1,4,6,16,17]. (See Draper [7] for a more comprehensive review of glass occurrences and models for their origins.) Despite this controversy, there is an emerging consensus that the occurrence of glass in spinel peridotite xenoliths is related in some way to metasomatic processes that have enriched the xenoliths prior to their removal from the lithosphere and their transport to the surface. It is therefore important to understand this relationship, before using the glasses to make inferences about metasomatic enrichment, or about other processes that may have operated in the lithosphere.

Using a LA–ICP–MS system at the Australian National University, we have analysed the trace element compositions of glasses and associated metasomatic phases (amphibole, phlogopite, apatite and clinopyroxene) from an extensively documented suite of mantle-derived spinel peridotite xenoliths from southeastern Australia [17–19]. These data are used here to further constrain the origin of the glassy patches present.

## 2. Sample descriptions and histories

The samples were hosted by the Newer Volcanics in southeastern Australia, and are glass ± amphibole ± phlogopite ± apatite-bearing spinel wehrlites, lherzolites and harzburgites. Petrographic occurrences of glassy patches and other phases have been previously described in detail [16,18,19]. Of 22 samples, 11 are spinel wehrlites, 6 are spinel lherzolites, and 5 are spinel harzburgites. All 22 samples contain patches and veinlets of glass, 16 contain apatite, only 4 contain pargasitic amphibole, and 3 contain phlogopite, which is invariably associated with amphibole. Sample lithologies and locations are presented in Table 1.

Table 1
Sample numbers, lithologies and localities within the Newer Volcanic Province of southeastern Australia, of the xenoliths comprising this study

| Sample | Lithology | Locality |
|---|---|---|
| 76991 | ApGlSpWEH | Mt Leura |
| SH15 | CbGlSpWEH | Mt Shadwell |
| SH35 | CbGlSpWEH | Mt Shadwell |
| SH45 | CbGlSpWEH | Mt Shadwell |
| SH61 | CbGlSpWEH | Mt Shadwell |
| 76988 | ApGlSpWEH | Mt Shadwell |
| 70972 | ApGlSpWEH | Mt Shadwell |
| 71000 | ApAmGlSpWEH | Mt Leura |
| 70965 | GlSpWEH | Mt Shadwell |
| 71001 | ApGlSpWEH | Mt Leura |
| 76987 | ApGlWEH | The Anakies |
| SH64 | CbGlSpLHZ | Mt Shadwell |
| 70987 | ApAmPhGlSpLHZ | Mt Leura |
| 71004 | ApAmPhGlSpLHZ | Mt Leura |
| 71006 | ApAmPhGlSpLHZ | Mt Leura |
| 71008 | ApGlSpLHZ | Mt Leura |
| 76994 | ApGlSpLHZ | Mt Leura |
| 71023 | ApGlSpHZ | Mt Leura |
| 76995 | CbApGlSpHZ | Mt Shadwell |
| 76997 | ApGlSpHZ | Mt Shadwell |
| 76998 | ApGlSpHZ | Mt Shadwell |
| 71003 | ApGlSpHZ | Mt Leura |

Ap = apatite; Gl = glassy patches; Sp = spinel; Cb = calcitic carbonate; Am = pargasitic amphibole; Ph = phlogopite; WEH = wehrlite; LHZ = lherzolite; HZ = harzburgite.

The xenoliths are inferred to have been very refractory residues (probably refractory lherzolites and harzburgites) produced by ancient extraction of picritic to basaltic melts during partial melting of more primitive, fertile peridotite [19,20], which were subsequently metasomatised by sodic dolomitic carbonatite melts, and possibly by other metasomatic agents [18]. Metasomatism resulted in partial to complete replacement of primary orthopyroxene in the residual peridotite by sodic clinopyroxene, and in crystallisation of accessory amphibole, apatite and phlogopite [18]. Addition of at least 6–12 wt% sodic dolomitic carbonatite melt (composition of Wallace and Green [21]) to refractory lithosphere could have generated the observed wehrlite whole-rock compositions, whereas the lherzolites require ∼8%, and the harzburgites require minimal or no carbonatite

addition [19,22]. The metasomatically enriched fragments of the lithosphere were later accidentally entrained as xenoliths in alkalic magmas during magmatism related to eruption of the Tertiary to Recent Newer Volcanics.

Yaxley et al. [16] proposed the following model to explain the occurrence of glass in this strongly metasomatised suite. Metasomatically introduced phases (amphibole, phlogopite, apatite and clinopyroxene) melted partially, either in the lithospheric wall-rock adjacent to intruding magmas, or after entrainment into those magmas, to form intergranular pockets of melt. The melts derived from breakdown of metasomatic phases were modified by crystallisation of a secondary assemblage of clinopyroxene + spinel ± olivine microlites, and in the lherzolites and harzburgites, by reaction with primary orthopyroxene [16]. Upon eruption, the modified melt pockets and veins quenched to form the observed glassy patches.

## 3. Sample preparation and analytical techniques

Preparation of samples for LA–ICP–MS analysis involved coarse-crushing of fragments of 22 xenoliths to liberate individual mineral grains and glassy patches. Glassy patches, and individual grains of clinopyroxene, amphibole, phlogopite and apatite were obtained by handpicking from the crushed xenoliths. These grain separates were mounted in epoxy and polished.

Trace element analyses of glassy patches, and metasomatic mineral phases (clinopyroxene, amphibole, apatite, phlogopite) were obtained using the LA–ICP–MS system at the Research School of Earth Sciences (The Australian National University). This system employs an ArF Excimer laser, which ablates sample material in a sample chamber and carries the plasma into a Fisons PQ2 STE ICP–MS instrument. This system is described in detail by Eggins et al. [17,23].

Our analytical protocol consisted of analysing a standard glass (NIST 610) at the commencement of each session, and at regular intervals during the session (i.e. after every 4–9 analyses of unknowns), and at the end of each session. We also analysed $^{43}$Ca and $^{49}$Ti as internal reference isotopes for data reduction.

Following ablation of small volumes of each analysed grain using LA–ICP–MS, the grain mounts were repolished and carbon-coated, and major and minor element analyses were obtained using either a Cameca SX50 electron probe microanalyser (WDS analyses), or a JEOL 6400 scanning electron microscope fitted with a Link energy dispersive detector. For each grain subjected to LA–ICP–MS analysis, replicate major and minor element electron probe microanalyses (EPMA) were obtained from close proximity to the ablated laser pit in the grain surface, in order to minimise potential uncertainty during reduction of the trace element data caused by possible compositional heterogeneity in the sample grains. Representative major, minor and trace element analyses of glasses and metasomatic phases are presented in Tables 2–4. We used the reference elements Ca in apatite, amphibole, clinopyroxene and glass, and Ti in phlogopite, as determined by EPMA, for reducing the LA–ICP–MS spectra, following the method described by Eggins et al. [17,23]. Typical analytical precision ($2\sigma$) for elements analysed by LA–ICP–MS was <2% for Ti, Sr and Ba, 2–5% for Sc, V, Y, Zr, Nb, La and Ce, 5–10% for Rb, Nd, Eu, Gd, Er, Yb, Hf, Ta and Th, and 10–15% for Sm, Lu, Pb and U. Detection limits were less than 0.10 ppm for most analysed trace elements (see Tables 2–4). Detection limits for minor elements analysed by EPMA were 0.10 wt% for $K_2O$, $TiO_2$ and MnO, 0.15 wt% for $Na_2O$ and $Cr_2O_3$, and 0.25 wt% for $P_2O_5$.

## 4. Trace element compositions of glasses and metasomatically introduced phases

### 4.1. Glass

We obtained trace element analyses of 1 to 4 different glassy patches from each of 22 samples. Major, minor and trace element analyses of some of the glasses are presented in Table 2, with representative primitive mantle (PM) normalised [24] trace element diagrams in Fig. 1. Our full data set, including analyses of glasses and metasomatic phases is available in the **EPSL Online Background Dataset** [1]. All glasses (with the exception of some patches from

[1] http://www.elsevier.nl/locate/epsl, mirror site: http://www.elsevier.com/locate/epsl

Table 2
Representative major and minor element oxide (wt%) and trace element (ppm) analyses of glasses

| Element | 76991 | 76991 | SH15 | SH35 | 70972 | 71000 | 76988 | 76994 | 76995 |
|---|---|---|---|---|---|---|---|---|---|
| $SiO_2$ | 51.76 | 53.21 | 50.63 | 49.73 | 52.34 | 49.80 | 51.31 | 52.63 | 60.72 |
| $TiO_2$ | 1.12 | 0.84 | 1.96 | 1.63 | 1.96 | 0.75 | 0.94 | 1.47 | 2.50 |
| $Al_2O_3$ | 21.34 | 20.69 | 20.28 | 19.66 | 20.24 | 21.52 | 21.26 | 17.38 | 14.91 |
| FeO | 3.34 | 3.20 | 4.11 | 3.34 | 4.66 | 3.40 | 3.12 | 3.46 | 2.77 |
| MnO | <0.10 | <0.10 | 0.27 | <0.10 | 0.17 | <0.10 | <0.10 | 0.16 | 0.16 |
| MgO | 2.19 | 2.19 | 2.37 | 2.60 | 2.13 | 3.85 | 2.65 | 4.08 | 1.93 |
| CaO | 4.56 | 2.84 | 5.04 | 4.91 | 4.75 | 7.56 | 5.31 | 7.14 | 2.81 |
| $Na_2O$ | 11.16 | 12.13 | 8.44 | 6.88 | 6.77 | 9.11 | 8.79 | 9.12 | 6.22 |
| $K_2O$ | 2.39 | 2.16 | 4.00 | 6.45 | 6.52 | 2.58 | 2.58 | 3.26 | 3.31 |
| $P_2O_5$ | <0.25 | <0.25 | 0.78 | 1.35 | 0.75 | 1.40 | 0.29 | 1.47 | 0.83 |
| $Cr_2O_3$ | <0.15 | 0.19 | <0.15 | <0.15 | <0.15 | <0.15 | 0.25 | <0.15 | <0.15 |
| Total | 98.05 | 97.57 | 97.91 | 96.70 | 100.30 | 100.06 | 96.50 | 100.24 | 96.17 |
| Sc | 6.36 | 3.94 | 4.14 | 3.86 | 3.86 | 9.12 | 5.09 | 22.9 | 12.9 |
| Ti | 7342 | 5675 | 10984 | 7620 | 7603 | 4175 | 5241 | 9578 | 12180 |
| V | 376 | 244 | 145 | 129 | 73.7 | 190 | 126 | 248 | 72.0 |
| Rb | 11.2 | 7.81 | 71.8 | 125 | 112 | 22.3 | 11.6 | 86.2 | 30.6 |
| Sr | 1573 | 1435 | 821 | 1534 | 1125 | 1309 | 1053 | 2306 | 256 |
| Y | 26.1 | 25.1 | 21.9 | 19.9 | 23.9 | 25.9 | 19.7 | 60.4 | 20.7 |
| Zr | 543 | 494 | 453 | 323 | 222 | 352 | 487 | 90.3 | 360 |
| Nb | 900 | 664 | 445 | 147 | 325 | 467 | 1088 | 38.6 | 164 |
| Ba | 589 | 387 | 659 | 5948 | 3363 | 527 | 731 | 1432 | 604 |
| La | 28.8 | 32.0 | 55.2 | 126 | 65.4 | 68.2 | 27.4 | 412 | 65.1 |
| Ce | 90.1 | 92.1 | 114 | 212 | 141 | 159 | 87.3 | 723 | 141 |
| Nd | 50.6 | 47.3 | 46.5 | 61.1 | 58.8 | 70.1 | 47.2 | 215 | 56.5 |
| Sm | 9.80 | 9.97 | 8.29 | 8.51 | 10.4 | 12.0 | 8.72 | 28.4 | 9.18 |
| Eu | 3.60 | 3.22 | 2.69 | 2.56 | 3.43 | 3.70 | 2.92 | 8.28 | 2.02 |
| Gd | 7.49 | 7.42 | 6.68 | 5.72 | 7.23 | 8.69 | 6.25 | 18.77 | 6.71 |
| Dy | 5.84 | 5.92 | 4.87 | 3.97 | 5.15 | 5.62 | 4.32 | 12.2 | 4.61 |
| Er | 2.28 | 2.36 | 1.97 | 1.78 | 2.16 | 2.35 | 1.94 | 4.73 | 1.98 |
| Yb | 1.78 | 1.71 | 1.58 | 1.48 | 1.73 | 1.89 | 1.38 | 3.17 | 1.60 |
| Lu | 0.200 | 0.253 | 0.210 | 0.208 | 0.212 | 0.252 | 0.176 | 0.418 | 0.206 |
| Hf | 5.46 | 5.92 | 7.09 | 5.04 | 3.45 | 4.31 | 3.83 | 2.11 | 9.56 |
| Ta | 24.4 | 19.9 | 19.4 | 7.61 | 14.9 | 18.4 | 28.9 | 1.74 | 8.96 |
| Pb | 7.02 | 6.81 | 8.10 | 10.2 | 4.19 | 6.40 | 7.41 | 7.27 | 11.1 |
| Th | 1.01 | 1.11 | 7.81 | 17.1 | 7.18 | 7.07 | 1.65 | 36.4 | 10.1 |
| U | 0.239 | 0.329 | 2.35 | 4.97 | 2.05 | 1.46 | 0.321 | 7.47 | 2.94 |

sample 71023) are enriched above estimated PM values in all analysed incompatible trace elements, and the degree of enrichment is extremely variable from one sample to the next. For example, PM-normalised La/Yb [$(La/Yb)_{PM}$] varies from 4.7 to 94.1, Th from 0.41 to 45 ppm (4.8–531 × PM), and Ba from 103 to 5974 ppm (14.7–855 × PM). Glasses from different patches within individual samples generally exhibit small compositional variations compared with that exhibited by the entire suite.

Superimposed on the overall enrichment in incompatible trace elements are a number of unusual interelement fractionations. For example, a feature of glass patches from the majority of the samples (e.g. samples 76988, 76998, 71000, 70972, SH15, LE17, and SH45 and others) is a distinctive enrichment, on a PM-normalised basis, in Nb and Ta compared with elements of similar incompatibility (e.g. U, Th, K and La), resulting in very low U/Nb values (down to $3 \times 10^{-4}$, cf. 0.03 for PM). This contrasts with some other samples (e.g. 71023, 76994), in which Nb and Ta are strongly depleted in comparison with U and K or La, leading to high U/Nb (up to 0.5). These samples also exhibit strong relative depletions

Table 3
Representative major and minor element oxide (wt%) and trace element (ppm) analyses of clinopyroxene grains

| Element | 76991 | SH15 | SH35 | SH45 | SH61 | 70972 | 71000 | 70965 | 71001 | SH64 | 70987 | 71008 | 71003 |
|---|---|---|---|---|---|---|---|---|---|---|---|---|---|
| $SiO_2$ | 55.32 | 54.89 | 54.06 | 55.13 | 54.75 | 55.51 | 54.39 | 54.53 | 55.86 | 54.85 | 54.65 | 55.25 | 53.80 |
| $TiO_2$ | <0.10 | 0.10 | 0.14 | <0.10 | <0.10 | <0.10 | <0.10 | 0.10 | <0.10 | 0.14 | <0.10 | <0.10 | <0.10 |
| $Al_2O_3$ | 3.36 | 2.34 | 3.26 | 3.07 | 3.55 | 2.92 | 4.70 | 2.93 | 1.80 | 3.30 | 3.06 | 3.17 | 3.86 |
| FeO | 2.67 | 2.41 | 2.05 | 2.42 | 2.62 | 2.29 | 2.69 | 2.61 | 2.72 | 2.04 | 2.29 | 2.89 | 1.74 |
| MnO | 0.12 | 0.13 | <0.10 | 0.10 | <0.10 | 0.11 | <0.10 | <0.10 | <0.10 | <0.10 | 0.10 | 0.15 | <0.10 |
| MgO | 15.24 | 16.15 | 16.13 | 15.76 | 16.14 | 16.63 | 15.46 | 16.05 | 14.99 | 16.22 | 16.08 | 15.82 | 15.77 |
| CaO | 19.89 | 21.35 | 20.85 | 20.15 | 20.62 | 20.51 | 19.75 | 20.65 | 19.78 | 21.56 | 20.13 | 20.11 | 21.35 |
| $Na_2O$ | 2.34 | 1.50 | 1.63 | 2.10 | 1.50 | 1.85 | 2.35 | 1.91 | 2.47 | 1.44 | 1.75 | 1.86 | 1.54 |
| $Cr_2O_3$ | 1.70 | 0.89 | 1.62 | 1.58 | 1.41 | 1.58 | 1.55 | 1.30 | 3.30 | 1.10 | 1.89 | 1.57 | 1.01 |
| Total | 100.69 | 99.77 | 99.73 | 100.35 | 100.71 | 101.43 | 100.97 | 100.09 | 101.05 | 100.70 | 100.04 | 100.87 | 99.16 |
| Sc | 58.0 | 47.3 | 64.5 | 61.6 | 49.4 | 69.2 | 44.6 | 50.0 | 58.0 | 58.1 | 72.8 | 54.1 | 98.7 |
| Ti | 395 | 607 | 758 | 283 | 463 | 139 | 265 | 613 | 231 | 742 | 302 | 169 | 358 |
| V | 198 | 165 | 181 | 206 | 188 | 171 | 174 | 183 | 177 | 170 | 197 | 176 | 231 |
| Rb | <0.2 | | <0.2 | <0.2 | <0.2 | <0.2 | | <0.2 | | <0.2 | <0.2 | | <0.2 |
| Sr | 438 | 221 | 407 | 382 | 300 | 505 | 364 | 363 | 607 | 340 | 440 | 472 | 362 |
| Y | 16.1 | 13.0 | 16.3 | 16.8 | 14.0 | 25.0 | 17.7 | 15.4 | 30.2 | 11.2 | 24.0 | 20.8 | 5.4 |
| Zr | 190.1 | 184.0 | 196.7 | 136.2 | 97.2 | 76.2 | 136.2 | 258.0 | 202.5 | 184.7 | 169.5 | 76.7 | 6.2 |
| Nb | 0.74 | 1.00 | 0.78 | 1.58 | 0.77 | 1.96 | 0.45 | 0.88 | 0.37 | 1.38 | 0.30 | 0.32 | 0.08 |
| Ba | 0.24 | 0.13 | 4.82 | 0.28 | 0.19 | 0.55 | 0.25 | 0.22 | 0.32 | 1.23 | 0.37 | 0.30 | 0.53 |
| La | 8.08 | 5.15 | 20.75 | 11.76 | 9.53 | 12.86 | 9.75 | 7.76 | 11.63 | 12.54 | 14.38 | 15.73 | 18.63 |
| Ce | 31.30 | 20.84 | 53.46 | 40.42 | 35.75 | 48.04 | 35.26 | 28.98 | 44.78 | 34.93 | 49.55 | 51.39 | 45.73 |
| Nd | 26.28 | 19.32 | 30.75 | 29.33 | 25.75 | 39.96 | 27.24 | 24.63 | 37.87 | 23.39 | 37.37 | 35.59 | 18.81 |
| Sm | 6.44 | 5.08 | 6.24 | 6.67 | 6.02 | 9.61 | 6.54 | 6.13 | 10.26 | 5.13 | 8.65 | 7.78 | 2.74 |
| Eu | 2.14 | 1.66 | 1.94 | 2.17 | 1.99 | 3.09 | 2.15 | 1.99 | 3.60 | 1.57 | 2.77 | 2.51 | 0.84 |
| Gd | 5.41 | 4.54 | 5.18 | 5.62 | 4.96 | 8.18 | 5.52 | 5.32 | 9.56 | 4.23 | 7.38 | 6.39 | 1.73 |
| Dy | 3.91 | 3.32 | 3.77 | 3.96 | 3.41 | 5.79 | 4.04 | 3.83 | 7.47 | 2.87 | 5.37 | 4.61 | 1.08 |
| Er | 1.50 | 1.26 | 1.57 | 1.56 | 1.29 | 2.29 | 1.67 | 1.45 | 2.68 | 1.04 | 2.15 | 1.90 | 0.49 |
| Yb | 1.12 | 0.90 | 1.23 | 1.16 | 0.95 | 1.69 | 1.33 | 1.07 | 1.68 | 0.74 | 1.58 | 1.45 | 0.46 |
| Lu | 0.15 | 0.13 | 0.17 | 0.16 | 0.12 | 0.24 | 0.19 | 0.15 | 0.21 | 0.10 | 0.22 | 0.21 | 0.07 |
| Hf | 2.78 | 3.56 | 4.92 | 1.40 | 1.16 | 0.80 | 1.90 | 5.23 | 1.78 | 5.12 | 3.66 | 0.47 | 0.18 |
| Ta | 0.09 | 0.12 | 0.14 | 0.16 | 0.15 | 0.30 | 0.06 | 0.15 | 0.03 | 0.24 | 0.04 | 0.03 | 0.01 |
| Pb | 1.70 | 1.32 | 1.95 | 1.60 | 0.99 | 1.53 | 1.50 | 1.77 | 2.54 | 1.16 | 1.42 | 1.27 | 3.22 |
| Th | 0.21 | 0.16 | 1.46 | 0.48 | 0.33 | 0.36 | 0.45 | 0.25 | 0.28 | 1.10 | 0.61 | 0.56 | 1.82 |
| U | 0.04 | 0.03 | 0.28 | 0.07 | 0.07 | 0.07 | 0.08 | 0.05 | 0.06 | 0.23 | 0.09 | 0.08 | 0.58 |

in other high field strength elements (HFSE) such as Zr, Hf and Ti, leading to very low values of Zr/Sm (1.8 for sample 71023 and 3.1 for sample 76994, cf. PM estimate of 25) and Ti/Eu (346 for sample 71023 and 1140 for sample 76994, cf. PM estimate of 7740; Fig. 2A). Other samples show minor or no enrichment in HFSE relative to elements of similar incompatibility, although these samples have high absolute abundances of these (and other) elements relative to PM (e.g. SH35, 71001; Fig. 1C).

Rb and Ba are present in varying abundances in the glasses. All but 7 of the glass analyses contain less than 2200 ppm Ba. The remaining 7, however, contain from 3000 to 6000 ppm Ba (samples SH35, SH64 and 70972). Most samples contain less than 40 ppm Rb, but a number of analyses have from 50 to 220 ppm Rb. The 7 high-Ba analyses also contained high Rb (>100 ppm) and high $K_2O$ (>6 wt%). Rb and Ba abundances are well and positively correlated with $K_2O$ contents, with glasses from the only three phlogopite-bearing samples (71004, 71006 and 70987) amongst the most enriched in all three elements (Fig. 2).

### *4.2. Clinopyroxene*

The samples contained both coarse-grained clinopyroxene, most of which is believed to have

Table 4
Representative major and minor element oxide (wt%) and trace element (ppm) analyses of apatite, amphibole and phlogopite grains

| Element | Apatite | | | | | Amphibole | | | Phlogopite | | |
|---|---|---|---|---|---|---|---|---|---|---|---|
| | 76987 | 71001 | 71004 | 71008 | 71000 | 70987 | 71006 | 71000 | 70987 | 71004 | 71006 |
| $SiO_2$ | 0.71 | 1.11 | 0.59 | 0.60 | 0.52 | 43.32 | 44.01 | 44.56 | 38.49 | 38.82 | 39.24 |
| $TiO_2$ | 0.10 | <0.10 | 0.16 | <0.08 | 0.11 | 4.83 | 1.06 | 0.85 | 3.79 | 4.46 | 1.58 |
| $Al_2O_3$ | na | na | na | na | na | 13.09 | 14.10 | 13.56 | 16.09 | 15.43 | 15.99 |
| $Cr_2O_3$ | na | na | na | na | na | 1.24 | 1.76 | 2.43 | 0.59 | 0.74 | 1.16 |
| FeO | 0.63 | 0.65 | 0.47 | 0.50 | 0.72 | 3.52 | 4.30 | 3.62 | 3.75 | 3.53 | 4.21 |
| MnO | na | na | na | na | na | <0.09 | <0.10 | <0.10 | <0.09 | <0.09 | <0.09 |
| MgO | 0.60 | 0.47 | 0.30 | 0.66 | 0.69 | 16.83 | 17.15 | 17.52 | 21.76 | 21.88 | 22.81 |
| CaO | 52.66 | 49.53 | 51.93 | 51.51 | 50.07 | 11.33 | 10.80 | 10.86 | <0.06 | <0.06 | <0.06 |
| $Na_2O$ | <0.14 | <0.15 | <0.15 | <0.15 | <0.15 | 3.30 | 3.58 | 3.79 | 1.24 | 1.25 | 1.38 |
| $K_2O$ | <0.10 | <0.05 | 0.16 | 0.10 | <0.10 | 1.32 | 1.06 | 1.10 | 8.83 | 8.63 | 8.74 |
| $P_2O_5$ | 39.63 | 38.02 | 39.52 | 39.73 | 38.35 | na | na | na | na | na | na |
| Cl | 0.99 | 1.99 | 1.53 | 1.37 | 1.75 | na | na | na | na | na | na |
| Total | 95.30 | 91.76 | 94.66 | 94.47 | 92.21 | 98.78 | 97.81 | 98.27 | 94.53 | 94.73 | 95.11 |
| Sc | 1.98 | <1 | 2.26 | 1.43 | 1.64 | 45.2 | 48.6 | 35.1 | 9.77 | 5.10 | 7.34 |
| Ti | 30.1 | <4 | 104 | 37.6 | 5.42 | 36957 | 6376 | 4650 | 22400 | 25317 | 8620 |
| V | 29.5 | 0.791 | 1.14 | 1.20 | 1.04 | 378 | 380 | 313 | 198 | 169 | 214 |
| Rb | 0.396 | <0.3 | 0.427 | 0.397 | 0.451 | 7.21 | 7.02 | 3.62 | 384 | 355 | 443 |
| Sr | 10004 | 20546 | 11079 | 11385 | 10961 | 936 | 798 | 661 | 281 | 298 | 258 |
| Y | 230 | 410 | 181 | 212 | 164 | 34.4 | 28.0 | 23.0 | <0.1 | 0.178 | 0.368 |
| Zr | 34.1 | 2.75 | 10.5 | 8.89 | 5.62 | 150 | 86.0 | 182 | 46.0 | 11.7 | 15.0 |
| Nb | 1.17 | 0.13 | 2.01 | 1.39 | 0.16 | 50.0 | 50.0 | 184 | 84.6 | 71.2 | 62.7 |
| Ba | 197 | 223 | 184 | 94 | 141 | 360 | 357 | 227 | 3963 | 4914 | 3547 |
| La | 2707 | 2676 | 1857 | 2417 | 1645 | 30.4 | 24.4 | 17.3 | 0.099 | 0.100 | 0.190 |
| Ce | 4348 | 4897 | 3127 | 4078 | 2893 | 79.9 | 68.1 | 55.8 | 0.096 | 0.077 | 0.821 |
| Nd | 1368 | 1847 | 1085 | 1364 | 1015 | 57.1 | 43.4 | 41.0 | 0.287 | 0.410 | 0.740 |
| Sm | 172 | 284 | 147 | 179 | 131 | 14.6 | 10.0 | 9.2 | 0.316 | 0.280 | 0.346 |
| Eu | 40.7 | 74.4 | 36.7 | 42.6 | 32.3 | 4.16 | 2.85 | 3.02 | 0.106 | 0.159 | 0.102 |
| Gd | 104 | 192 | 89.6 | 104 | 80.9 | 11.9 | 7.96 | 7.75 | 0.162 | 0.170 | 0.201 |
| Dy | 55.5 | 105 | 43.1 | 51.7 | 40.5 | 8.55 | 6.02 | 5.38 | 0.149 | 0.127 | 0.204 |
| Er | 19.2 | 30.9 | 13.7 | 16.8 | 13.1 | 2.95 | 2.49 | 2.12 | 0.117 | 0.081 | 0.121 |
| Yb | 11.9 | 15.4 | 7.6 | 10.0 | 7.9 | 2.24 | 2.02 | 1.58 | 0.091 | 0.086 | 0.124 |
| Lu | 1.52 | 1.63 | 0.94 | 1.21 | 1.01 | 0.275 | 0.268 | 0.177 | 0.030 | 0.023 | 0.034 |
| Hf | 0.161 | 0.027 | 0.067 | 0.049 | 0.030 | 4.22 | 1.83 | 2.67 | 1.02 | 0.149 | 0.300 |
| Ta | 0.008 | 0.010 | 0.023 | 0.017 | 0.008 | 2.72 | 1.33 | 6.53 | 4.58 | 2.94 | 2.62 |
| Pb | 10.6 | 60.4 | 2.9 | 19.3 | 30.7 | 4.63 | 3.81 | 2.95 | 4.58 | 3.35 | 4.35 |
| Th | 400 | 293 | 198 | 254 | 214 | 2.55 | 1.43 | 1.08 | 0.024 | 0.021 | 0.031 |
| U | 76.9 | 74.8 | 38.5 | 47.1 | 40.5 | 0.409 | 0.319 | 0.197 | 0.031 | 0.019 | 0.043 |

been metasomatically introduced [19], and clinopyroxene microphenocrysts which crystallised from the glassy patches [16]. Ablation of some coarse-grained clinopyroxene resulted in extreme variations in count rates during analysis time for many isotopes, producing spectra which could not be satisfactorily reduced. This is a consequence of the presence of abundant tiny inclusions of glass and mineral phases such as amphibole, orthopyroxene, phlogopite, apatite and carbonate [19]. Data from spectra such as these are not considered further in this contribution. Similarly, we were unable to satisfactorily analyse clinopyroxene microphenocrysts present in the glassy patches, due to their small size, and to the ubiquitous presence of tiny inclusions of glass and Cr-spinel microlites.

However, in 24 grains from 13 samples, satisfactory spectra were obtained. Major, minor and trace element analyses of some clinopyroxene grains are presented in Table 3 and as representative PM-normalised trace element diagrams in Fig. 3. Analyses

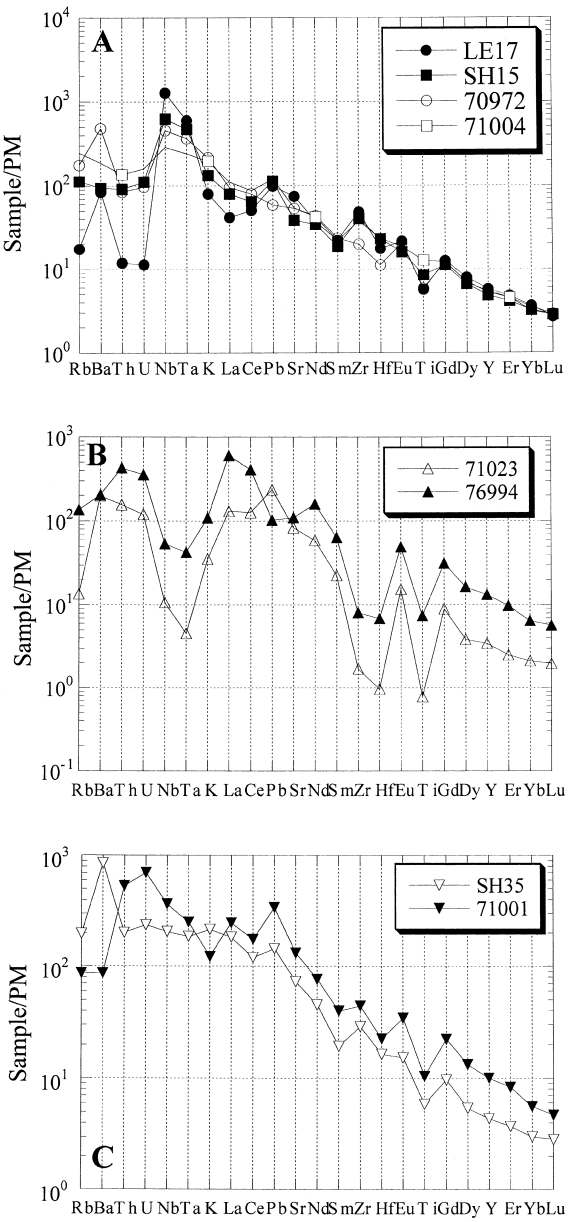


Fig. 1. Primitive mantle-normalised trace element diagrams for glasses exhibiting (A) enrichment in Nb and Ta over U, Th and K, (B) strong depletions in HFSE relative to LILE and REE, and (C) minor or no enrichments or depletions in HFSE relative to LILE or REE of similar incompatibility. Normalising values are those of [24]. See text for further explanation.

of different grains from individual samples, and from the entire suite exhibited similar abundance levels and gave very similar PM-normalised patterns. The

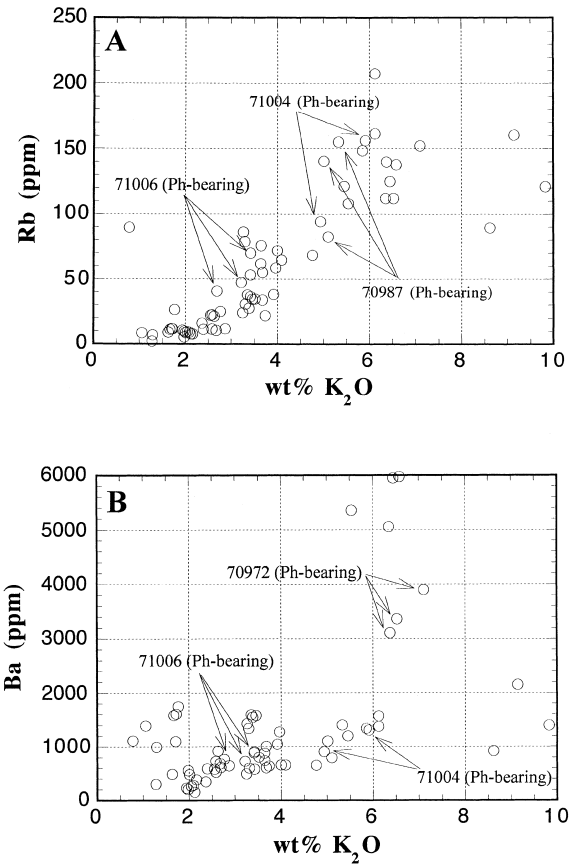


Fig. 2. (A) Rb (ppm) vs. $K_2O$ (wt%), and (B) Ba (ppm) vs. $K_2O$ (wt%), for glasses, with those glasses from phlogopite-bearing samples indicated.

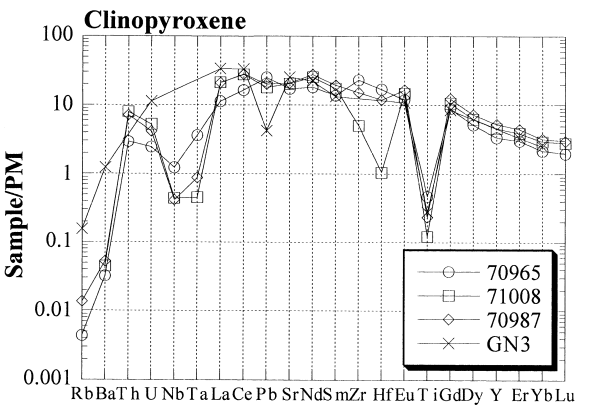


Fig. 3. Primitive mantle-normalised trace element diagram for representative coarse-grained clinopyroxene from three samples (*70965*, *71008* and *70987*) from the current suite. *GN3* is clinopyroxene analysis from [25].

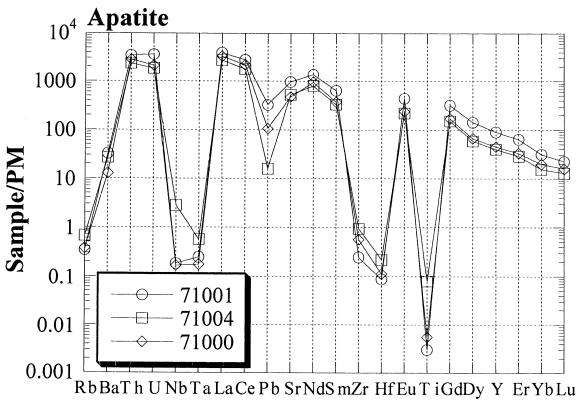


Fig. 4. Primitive mantle-normalised trace element diagram for representative apatites from three samples from the current suite.

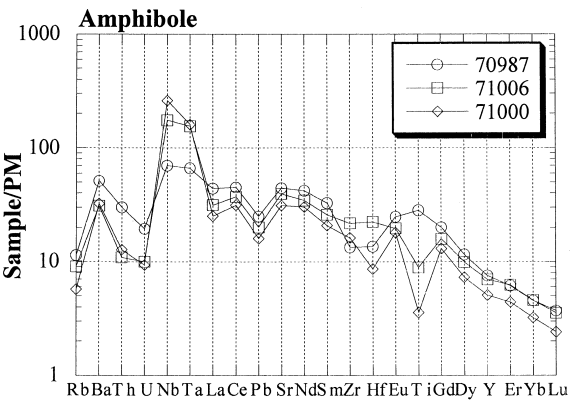


Fig. 5. Primitive mantle-normalised trace element diagram for representative amphibole from three samples from the current suite.

grains exhibited enrichments above PM values for U, Th, Pb, Sr, Zr and rare earth elements (REE). For example, La contents varied from 7.1 to 30.2 × PM. In contrast, Rb contents were often below detection limits, and Ba abundances were <0.6 ppm in most grains. Heavy rare earth element (HREE) contents were typically around 1–3 × PM. Despite the moderate enrichments in large-ion lithophile elements (LILE), Nb, Ta and Ti (HFSE) were markedly depleted or present in similar abundances to PM. This resulted in ubiquitous strong negative Ti anomalies on PM-normalised trace element spidergrams (with Ti always less than 0.6 × PM abundances), and in moderate to strong negative anomalies for Nb and Ta, and in some cases Hf. Thus clinopyroxenes exhibit some unusual interelement fractionations, with low Ti/Eu (45–673) and high La/Nb (5.1–50.9), Zr/Hf (21.5–174) and U/Nb (0.02–7.2).

The trace element patterns for clinopyroxenes from this suite are very similar to other reported apatite-bearing spinel peridotite xenoliths from southeastern Australia [25], and from Yemen [6,26] (Fig. 3).

### 4.3. Apatite

Apatite analyses from five samples were obtained, and some examples are presented in Table 4. PM-normalised diagrams are presented in Fig. 4. Individual apatite grains exhibit very similar trace element spectra, with extremely high concentrations of Th, U, and LREE (>1000 × PM), high concentrations of Sr, Nd and Sm (100–1000 × PM) and moderate concentrations of HREE (10–100 × PM). HFSE, as well as Rb and Ba were extremely low in abundance. This decoupling of LILE and REE from HFSE produced extremely low values for Ti/Eu (<12, cf. 7740 for PM), and extremely high values for Sm/Zr (up to 590, cf. 0.05 for PM) and U/Nb (up to 813, cf. 0.03 for PM).

Trace element patterns which we obtained for apatites are very similar to those reported by Baker et al. [26] for apatite separated from a hydrous spinel lherzolite xenolith from Yemen, and to those determined by proton microprobe from other southeastern Australian spinel peridotite xenoliths [27].

### 4.4. Amphibole

We obtained nine analyses of pargasitic amphibole from three samples (70987, 71000 and 71006). Representative analyses are presented in Table 4. Amphiboles are moderately enriched, with most incompatible trace elements present at abundances between 10× and 100× estimated PM values (Fig. 5). For example, La ranges from 14.5 to 30.4 ppm (21.1–44.2 × PM), and $(La/Yb)_{PM}$ from 6.6 to 10.4. However, in all samples, Nb and Ta were enriched above LILE (e.g. Th, U) and LREE, leading to low values of La/Ta (range 2.4–18.4; mean 6.5) and U/Nb (range $1 \times 10^{-3}$–$8 \times 10^{-3}$; mean $2 \times 10^{-3}$) compared to the PM estimates of 16.8 and 0.03, respectively.

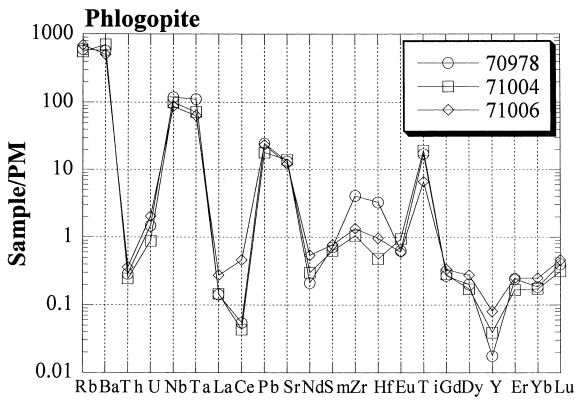


Fig. 6. Primitive mantle-normalised trace element diagram for representative phlogopite from three samples from the current suite.

Amphibole from samples 71000 and 71006 exhibited strong negative Ti anomalies on Fig. 5, leading to very low values of Ti/Eu (1375–3500, cf. 7740 for PM). This contrasts with amphibole from 70987, in which the Ti depletion relative to Eu is minor or absent. The two analysed amphibole grains from sample 70987 have Ti/Eu values of 8900 and 6900.

### *4.5. Phlogopite*

We analysed six phlogopite grains from three samples (70987, 71004 and 71006). Representative analyses are presented in Table 4. The trace element spectra (Fig. 6) of phlogopite exhibit the following features. Compared with estimated PM abundances, phlogopite grains are strongly enriched in Rb, Ba, Nb, Ta and Ti (usually $>40 \times$ PM), moderately enriched in Pb and Sr (usually 10–40 $\times$ PM), and slightly enriched or depleted in U, Th, REE and Y (Fig. 6). This leads to extremely high values for Ba/Th ($10^5$–$2.4 \times 10^5$, cf. 82 for PM), Sr/Nd (349–979, cf. 15.6 for PM) and Ti/Eu ($8.5 \times 10^4$–$2.6 \times 10^5$, cf. 7740 for PM), and very low U/Nb ($<10^{-3}$, cf. 0.03 for PM) and Ce/Pb (0.02–0.19, cf. 9.6 for PM).

## 5. Discussion

### *5.1. Sources of the glasses*

Yaxley et al. [16] suggested that the petrographic features, and the major and minor element geochemistry of the glassy patches and veins observed in the current suite, are the result of melting of metasomatic amphibole and clinopyroxene, with varying contributions of components derived from melting of other co-existing metasomatic phases (apatite, phlogopite and possibly an inferred Na-rich metasomatic component). This conclusion concurs with several other studies [1,6,17]. In the following discussion, we use the trace element data from the glasses and from the metasomatic phases to test this model for the origin of glass in the current xenolith suite.

The measured trace element compositions of the xenolith glasses cannot be directly related to those of formerly existing phases such as amphibole, due to the uncertain effects on glass compositions of the observed fractional crystallisation of microlites of olivine, clinopyroxene and spinel, and due to our inability to measure the compositions of clinopyroxene microlites. Furthermore, glasses in many samples have probably been modified towards higher $SiO_2$ contents by low-pressure reaction with primary orthopyroxene [16]. Given that orthopyroxene in mantle xenoliths is typically very substantially less enriched in most trace elements than clinopyroxene or glass [17], this reaction is likely to have diluted initial trace element abundances in the liquids which later quenched to form the glasses.

However, use of ratios of trace elements may allow discrimination between contributions to the glasses from the various metasomatic phases. For example, Fig. 7A is a plot of Ba/Th vs. Ce/Pb for glasses, amphibole, apatite, phlogopite and clinopyroxene, which illustrates a number of important points. Firstly, Ce/Pb for nine amphibole analyses from three samples is constant (mean $\pm$ $1\sigma = 19.9 \pm 2.2$) across a four-fold range of Ba/Th values (98–409). Many of the glasses fall within a restricted range of Ce/Pb; for example, 78% of glass analyses have Ce/Pb in the range 5–40. The remainder have values between 40 and 129. Clinopyroxenes have a similar range of Ce/Pb values to the majority of glasses (13.3–40.5), but significantly lower Ba/Th ($<3.3$). Most of the glasses have Ba/Th values similar to, or slightly less than the range exhibited by amphibole (i.e. $<400$), although a few analyses extend the range as high as 622. Thus, most glasses plot near amphibole, or between amphibole and clinopyroxene, on Fig. 7A.

Similarly, Fig. 7B is a plot of Ba/Th vs. Ti/Eu for glasses, and metasomatic phases. The clinopyroxenes have Ti/Eu < 700, and Ba/Th < 3, whereas amphibole grains have higher, but fairly constant Ti/Eu (~3000) and higher Ba/Th (100–300). Again, most of the glasses define a field which overlaps that of amphibole and extends towards the clinopyroxene field, although a small sub-set of glasses lies on the phlogopite side of the amphibole field.

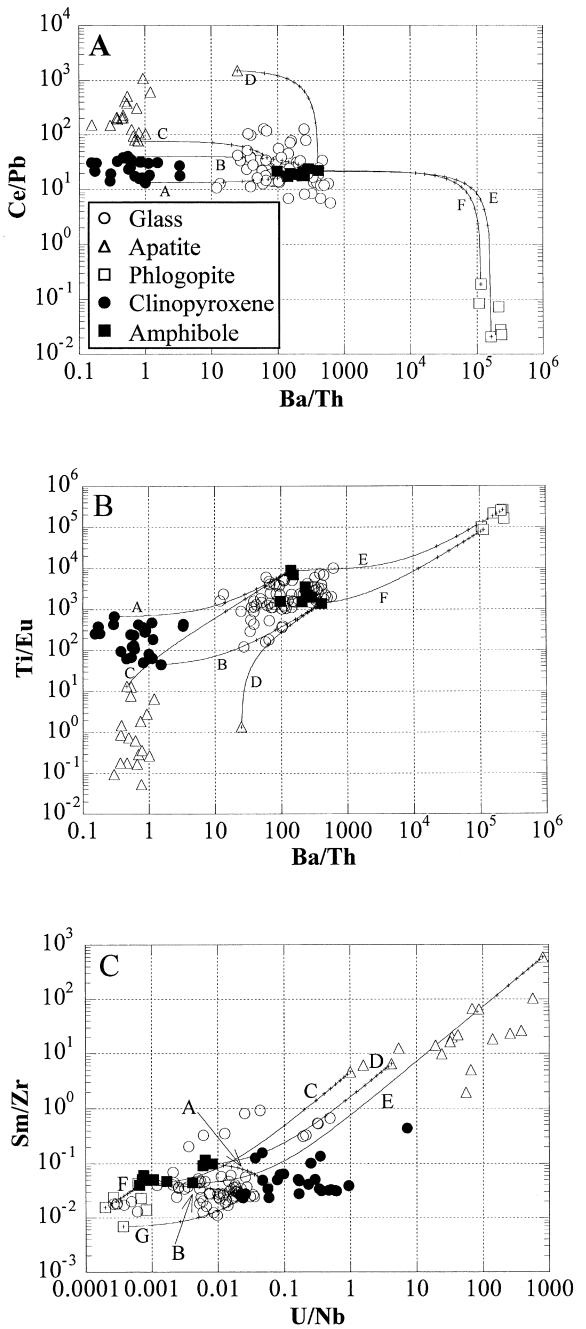


On a plot of U/Nb vs. Sm/Zr (Fig. 7C), most phlogopite, amphibole, glass and clinopyroxene analyses have Sm/Zr between 0.01 and 0.1, although a few glasses are substantially higher (up to 1.0). Apatite has still higher Sm/Zr (2–550). U/Nb is distinctive for each phase ($<10^{-3}$ for phlogopite, $6 \times 10^{-4}$–0.01 for amphibole, >0.04 for clinopyroxene, and >1 for apatite). Again, most glasses plot in a field that lies between, and overlaps fields for clinopyroxene and amphibole, with a small group of glass analyses having similar U/Nb and Sm/Zr values to phlogopite, and another small group extending the glass compositions towards those of apatite.

### 5.2. Mixing models

The ratio–ratio plots in Fig. 7 suggest that the majority of the glasses in this suite may be dominated by components derived from melting of amphibole and clinopyroxene. Those glasses with the highest values of Ce/Pb and Sm/Zr may contain additional components derived from partial melting of apatite or some other high Ce/Pb and Sm/Zr component(s), and those glasses with the lowest values of Sm/Zr and U/Nb, and highest Ba/Th may include components derived from breakdown of phlogopite. In order to test these interpretations, we have modelled mixing between melts with the compositions of amphibole, clinopyroxene, apatite, and phlogopite (Fig. 7). Our modelling assumes that melting is modal, i.e. the liquid trace element compositions

Fig. 7. (A) Ba/Th vs. Ce/Pb, (B) Ba/Th vs. Ti/Eu, and (C) U/Nb vs. Sm/Zr for glasses, amphibole, phlogopite, apatite and clinopyroxene. Mixing curves are for simple binary mixing between selected analyses of amphibole and clinopyroxene, amphibole and apatite, and amphibole and phlogopite. Crosses on mixing curves are 10% increments. These plots illustrate that glass compositions are consistent with mixing of components derived from modal melting of amphibole, usually with contributions from modal melts of clinopyroxene. Some glasses also require input of additional components from apatite or phlogopite. See text for further information.

were controlled by bulk addition of the various phases which melted and contributed to the melt pool, rather than by equilibrium partitioning relationships between liquid and relict, partially molten phases. The absence of amphibole (inferred to be a major contributor to most of the glasses) from all but four of our sample suite, and petrographic evidence for bulk dissolution of clinopyroxene [16,18,19], suggest that modal melting was a very significant control on glass compositions. Also, Tsuchiyama [28] has suggested on the basis of an experimental study of the kinetics of melting of diopside–plagioclase mineral pairs, that disequilibrium modal melting is likely to occur during partial melting of xenoliths being transported by magmas to the surface.

*5.2.1. Amphibole–clinopyroxene mixing*

On Fig. 7A, we have modelled bulk mixing between the amphibole and clinopyroxene analyses with the lowest Ce/Pb (mixing line A), and between those with the highest Ce/Pb (mixing line B). This range of potential mixing curves encompasses ~80% of the glass analyses, and suggests that most glass compositions are consistent with mixing between ~0 and 90% melt with the average bulk clinopyroxene composition and ~100 and 10% of melt with the average bulk amphibole composition. Similarly, nearly all glass compositions can also be satisfactorily modelled on Fig. 7B by modal mixing of ~10–90% amphibole and ~90–10% clinopyroxene (mixing lines A and B). On Fig. 7C, mixing lines A and B are also consistent with the many of these glasses being the product of mixing of varying amounts of melts with bulk amphibole compositions and bulk clinopyroxene compositions.

*5.2.2. Involvement of apatite?*

Ten glass analyses have Ce/Pb (Fig. 7A) and Sm/Zr (Fig. 7C) significantly higher than values along the amphibole–clinopyroxene mixing lines, apparently requiring additional input of a component with high Ce/Pb, Sm/Zr and U/Nb, possibly apatite. Five glass analyses from samples 76994 and 71023 have both Sm/Zr and U/Nb $> 0.1$, and define a clear mixing trend from the amphibole towards apatite (Fig. 7C, mixing line D). These glasses have compositions consistent with mixing of <10% of a liquid with a bulk apatite composition and >90% of liquid with a bulk amphibole composition. A further five glass analyses from sample 76987 have Sm/Zr $> 0.1$ but U/Nb between 0.002 and 0.05. We were unable to determine a mixing line for these samples between any of our measured amphibole or apatite compositions, although it is likely that these glasses could be the product of mixing between glass with an amphibole composition and glass with an apatite composition somewhat lower in U/Nb than any of the measured apatite compositions.

*5.2.3. Involvement of phlogopite?*

There is no evidence on Fig. 7A for involvement of phlogopite with similar composition to the compositions of phlogopite grains measured here, as none of the glass analyses lie on mixing lines between amphibole or any of the measured phlogopite compositions (Fig. 7A; mixing lines E and F). A small group of five glass analyses from phlogopite-free samples SH5, SH15 and 76997, have distinctly lower Ce/Pb (<10) than the remainder of the glass analyses, but do not lie on any mixing lines between amphibole and phlogopite, nor between clinopyroxene and phlogopite (Fig. 7A). We do not currently have a satisfactory explanation for the Ce/Pb and Ba/Th values of these glasses. However, on Fig. 7B, a few glasses plot to the higher Ti/Eu and Ba/Th side of the amphibole field (i.e. those with Ba/Th $> 230$), and extend the glass field slightly towards phlogopite, which has very high Ti/Eu and Ba/Th (both $> 10^5$). These glasses require only a few % addition of the phlogopite component to melts of amphibole composition (mixing lines E and F, Fig. 7B). Similarly, on Fig. 7C, another small group of glass analyses (i.e. those with Sm/Zr $< 0.02$) plot within the field for phlogopite, with extremely low values of both ratios, or have compositions consistent with mixing between melts with compositions of amphibole, clinopyroxene and phlogopite (Fig. 7C; mixing curves B, F and G). The glasses with Sm/Zr $< 0.02$ nearly all have high Ba/Th (>230) (Fig. 8), consistent with a contribution by phlogopite to their trace element compositions.

Thus, although the modelling cannot completely account for the complexities of the processes which modified the glasses after their formation, key trace element ratios are broadly consistent with derivation

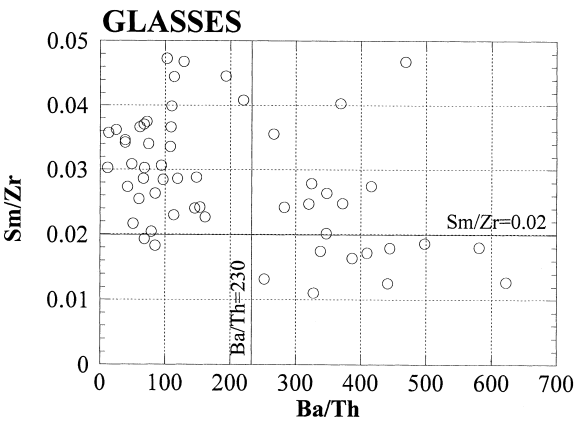


Fig. 8. Ba/Th vs. Sm/Zr for glasses from this suite. Note that most of the glasses with Sm/Zr < 0.02 have high Ba/Th (>230). This indicates that a component derived from phlogopite is present in these glasses. See text for further information.

of the majority of the analysed glasses by modal melting of amphibole and clinopyroxene, with added components in a few cases, from modal melting of phlogopite, or apatite. Nevertheless, we cannot absolutely preclude a role for partitioning relationships in partially controlling the trace element contributions to the glasses by phases which have not melted out completely (i.e. phases which have remained relict).

## 6. Conclusions

We conclude that the trace element data from glass in patches, and from the metasomatic phase assemblage (clinopyroxene + amphibole + phlogopite + apatite) strongly support our earlier model [16] (based on petrographic, major and minor element evidence) for the formation of glass in the southeastern Australian xenolith suite. Certain key trace element ratios (e.g. Sm/Zr, U/Nb, Ba/Th, Ce/Pb, Ti/Eu), considered to be relatively robust to alteration by microlite crystallisation or by reaction with orthopyroxene, exhibit large contrasts between the different phases which potentially contribute to the glass. On ratio–ratio plots, most glasses lie between, and overlap with, fields for amphibole and clinopyroxene, consistent with their derivation from breakdown (modal melting) of these phases. A few glasses probably contain a component derived from modal melting of phlogopite, and other glasses contain a component derived from modal melting of apatite. Trace element mixing models clearly cannot completely describe the complex variety of processes and sources which contributed to the final glass compositions, but do support the notion that these glasses are largely the products of disequilibrium processes involving modal melting (i.e. the liquid trace element compositions reflect bulk addition to the liquid pool of partially or completely molten phases, rather than equilibrium partitioning between liquid and relict phases) of a metasomatically introduced assemblage dominated by amphibole and clinopyroxene.

The glass-forming event clearly post-dates metasomatic addition of the contributing phases, and most probably occurred during transport and decompression of the xenoliths at magmatic temperatures, in the host magma. We emphasise that the large and variable fractionations between trace elements in the glasses are best explained as the result of varying contributions from a compositionally heterogeneous, pre-existing metasomatic assemblage to the liquids which ultimately quenched to form the glasses. The xenolith glasses therefore represent disequilibrium breakdown products of this pre-existing metasomatic assemblage, and not the metasomatic agent itself. However, despite the complexities of the formation and subsequent modification of the liquids which quenched to form the glasses in our suite, the trace element data from the glasses and mineral phases can be used to infer the former presence of amphibole in many of those xenoliths which are now amphibole-absent.

## Acknowledgements

VK was supported by an Australian Research Fellowship and Grant, and by the Australian Research Council's Research Centres Program and GMY by an Australian Research Council Postdoctoral Fellowship. Steve Eggins and Les Kinsley assisted with the LA–ICP–MS analyses. Nick Ware (The Australian National University), and David Steele and Wies Jablonski (University of Tasmania) helped with EPMA. David Green and Steve Eggins are thanked for discussions on various aspects of this work. The manuscript benefited from careful reviews by Drs.

Trevor Falloon, Andreas Klügel and an anonymous reviewer. ***[CL]***

## References


[1] F.A. Frey, D.H. Green, The mineralogy, geochemistry and origin of lherzolite inclusions in Victorian basanites, Geochim. Cosmochim. Acta 38 (1974) 1023–1059.

[2] A.P. Jones, J.V. Smith, J.B. Dawson, Glasses in mantle xenoliths from Olmani, Tanzania, J. Geol. 91 (1983) 167–178.

[3] D.S. Draper, Spinel lherzolite xenoliths from Lorena Butte, Simcoe Mountains, Southern Washington (USA), J. Geol. 100 (1992) 766–776.

[4] E.H. Hauri, N. Shimuzu, J.J. Dieu, S.R. Hart, Evidence for hotspot-related carbonatite metasomatism in the oceanic upper mantle, Nature 365 (1993) 221–227.

[5] E. Zinngrebe, S.F. Foley, Metasomatism in mantle xenoliths from Gees, West Eifel, Germany: evidence for the genesis of calc-alkaline glasses and metasomatic Ca-enrichment, Contrib. Mineral. Petrol. 122 (1995) 79–96.

[6] G. Chazot, M.A. Menzies, B. Harte, Determination of partition coefficients between apatite, clinopyroxene, amphibole, and melt in natural spinel lherzolites from Yemen: implications for wet melting of the lithospheric mantle, Geochim. Cosmochim. Acta 60 (1996) 423–437.

[7] D.S. Draper, T.H. Green, P–T phase relations of silicic, alkaline, aluminous mantle-xenolith glasses under anhydrous and C–O–H fluid-saturated conditions, J. Petrol. 38 (1997) 1187–1224.

[8] M.B. Baker, M.M. Hirschmann, M.S. Ghiorso, E.M. Stolper, Compositions of near-solidus peridotite melts from experiments and thermodynamic calculations, Nature 375 (1995) 308–311.

[9] R.J. Kinzler, C.H. Langmuir, Minute mantle melts, Nature 375 (1995) 274–275.

[10] E. Wulff-Pedersen, E.-R. Neumann, B.B. Jensen, The upper mantle under La Palma, Canary Islands: formation of Si–K–Na-rich melt and its importance as a metasomatic agent, Contrib. Mineral. Petrol. 125 (1996) 113–139.

[11] R. Vannucci, P. Bottazzi, E. Wulff-Pedersen, E.-R. Neumann, Partitioning of REE, Y, Sr, Zr and Ti between clinopyroxene and silicate melts in the mantle under La Palma (Canary Islands): implications for the nature of the metasomatic agents, Earth Planet. Sci. Lett. 158 (1998) 39–51.

[12] D.A. Ionov, A.W. Hofmann, N. Shimuzu, Metasomatism-induced melting in mantle xenoliths from Mongolia, J. Petrol. 35 (1994) 753–758.

[13] P. Schiano, R. Clocchiatti, J.L. Joron, Melt and fluid inclusions in basalts and xenoliths from Tahaa Island, Society Archipelago: evidence for a metasomatized upper mantle, Earth Planet. Sci. Lett. 111 (1992) 69–82.

[14] P. Schiano, R. Clocchiatti, Worldwide occurrence of silica-rich melts in sub-continental and sub-oceanic mantle minerals, Nature 368 (1994) 621–624.

[15] P. Schiano, R. Clocchiatti, N. Shimuzu, D. Weis, N. Mattielli, Cogenetic silica-rich and carbonate-rich melts trapped in mantle minerals in Kerguelen ultramafic xenoliths: implications for metasomatism in the oceanic upper mantle, Earth Planet. Sci. Lett. 123 (1994) 167–178.

[16] G.M. Yaxley, V. Kamenetsky, D.H. Green, T.J. Falloon, Glasses in mantle xenoliths from western Victoria, Australia, and their relevance to mantle processes, Earth Planet. Sci. Lett. 148 (1997) 433–446.

[17] S.M. Eggins, R.L. Rudnick, W.F. McDonough, The compositions of peridotites and their minerals: a laser-ablation ICP–MS study, Earth Planet. Sci. Lett. 154 (1998) 53–71.

[18] G.M. Yaxley, A.J. Crawford, D.H. Green, Evidence for carbonatite metasomatism in spinel peridotite xenoliths from western Victoria, Australia, Earth Planet. Sci. Lett. 107 (1991) 305–317.

[19] G. Yaxley, D. Green, V. Kamenetsky, Carbonatite metasomatism in the southeastern Australian lithosphere, J. Petrol. 39 (1998) 1917–1930.

[20] M.R. Handler, V.C. Bennett, T.M. Esat, The persistence of off-cratonic lithospheric mantle: Os isotopic systematics of variably metasomatised southeast Australian xenoliths, Earth Planet. Sci. Lett. 151 (1997) 61–75.

[21] M. Wallace, D.H. Green, An experimental determination of primary carbonatite composition, Nature 335 (1988) 343–345.

[22] G.M. Yaxley, D.H. Green, Experimental reconstruction of sodic dolomitic carbonatite melts from metasomatised lithosphere, Contrib. Mineral. Petrol. 124 (1996) 359–364.

[23] S.M. Eggins, L.K. Kinsley, J.M.G. Shelley, Deposition and element fractionation processes occurring during atmospheric pressure laser sampling for analysis by ICPMS, Appl. Surf. Sci. 129 (1998) 278–283.

[24] S.-s. Sun, W.F. McDonough, Chemical and isotopic systematics of oceanic basalts: implications for mantle composition and processes, in: A.D. Saunders, M.J. Norry (Eds.), Magmatism in the Ocean Basins, Special Publication, Geological Society of London, 1989, pp. 313–345.

[25] A.J. Stolz, G.R. Davies, Chemical and isotopic evidence from spinel lherzolite xenoliths for episodic metasomatism of the upper mantle beneath southeast Australia, J. Petrol. Special Lithosphere Issue (1988) 303–330.

[26] J. Baker, G. Chazot, M. Menzies, M. Thirlwall, Metasomatism of the shallow mantle beneath Yemen by the Afar plume — implications for mantle plumes, flood volcanism, and intraplate volcanism, Geology 26 (1998) 431–434.

[27] S.Y. O'Reilly, W.L. Griffin, C.G. Ryan, Residence of trace elements in metasomatized spinel lherzolite xenoliths: a proton-microprobe study, Contrib. Mineral. Petrol. 109 (1991) 98–113.

[28] A. Tsuchiyama, Partial melting kinetics of plagioclase–diopside pairs, Contrib. Mineral. Petrol. 91 (1985) 12–23.